U.S. Department of Commerce
National Oceanic and Atmospheric Administration
National Weather Service
National Centers for Environmental Prediction
5200 Auth Road
Camp Springs, MD 20746

NCEP Office Note 441

Parameterization of Solar Radiation Transfer in the NCEP Models

Yu-Tai Hou[1]
Shrinivas Moorthi
Kenneth Campana

October, 2002

[1]Corresponding Author E-mail: yu-tai.hou@noaa.gov

Abstract

This technical memorandum documents the solar radiation computation package currently used in NCEP's models. The solar radiative transfer model includes parameterizations of absorptions by various gases, clouds, and aerosols, as well as scattering by clouds, aerosols, and gas molecules. The document also discusses separately various techniques used in the parameterizations for atmospheric aerosol distributions and optical properties, cloud optical properties, and surface albedos.

1. Introduction:

Solar radiation is the most important source of energy to the earth-atmosphere system. Accurate calculation of this external energy source is therefore extremely important to understand and predict the dynamics and climate of the earth-atmosphere system. For computational efficiency reason, atmospheric general circulation models (GCM) generally use broadband parameterization method for solar radiation computations. In recent years, advances in improved techniques for radiative transfer calculation, parameterization of optical properties for cloud and aerosol, and surface albedo treatments have greatly improved the quality of weather prediction and climate change research. At NCEP, a new solar radiation parameterization package has become operational in the global forecast system (GFS) since 1995. This solar

radiation algorithm was developed largely based on Chou (1992), and has been since updated and improved several times following Chou and Lee (1996), and Chou and Suarez (1999). At the same time, improvements have been also done on other closely related parts of the models, such as parameterization of cloud-optical properties, atmospheric aerosols, and surface albedo, etc.

This technical memorandum is intended to document the solar radiation parameterization package used in NCEP's models. Section 2 gives a brief introduction of solar radiation transfer theory. Section 3 discusses the spectral band structures and the parameterization of atmospheric gases' absorptions. Section 4 describes Rayleigh scattering and the parameterization of aerosol effect. The parameterization of cloud optical properties is given in Section 5. Section 6 shows the detailed techniques used in radiation flux calculation, and Section 7 discusses the flux calculation in cloudy sky and the reduction of radiation flux due to CO_2 and O_2 absorptions. Finally, the parameterization of model surface albedo is explained in Section 8.

2. Solar radiation transfer theory:

Solar radiation spans a wide range of frequency spectrum, roughly from 0.2 μ to 4 μ. Figure 1 (from Stephens, 1984) shows the clear sky solar irradiance received at sea level. In the figure, two distinct spectral regions are separated around wavelength $\lambda = 0.7$ μ (wavenumber ν at 14280 cm^{-1}). In the ultraviolet and visible (UVV) spectral region ($\lambda < 0.7$ μ), atmospheric ozone is the primary absorber, while water vapor absorption dominates the near infrared (NIR) spectrum region ($\lambda > 0.7$ μ). Absorptions due to other gases, such as O_2 and CO_2 also present in

various spectral locations, but their contributions to the atmospheric heating are much smaller.

2.1 Simplified non-scattering atmosphere:

In a non-scattering atmosphere, the calculation of solar radiation transfer is straightforward. The downward radiation flux at height z of the atmosphere is expressed as Stephens (1984):

$$F^{\downarrow}(z,\mu_0) = \mu_0 \int_0^{\infty} S_{0\nu}\, T_{\nu}(u(z),\mu_0)\, d\nu \tag{2.1}$$

where $S_{o\nu}$ is the incident solar radiation beam at the top of the atmosphere for spectral frequency ν, μ_o is the cosine of the incident zenith angle θ_o, and u is the absorber amount along the path from z to the top of the atmosphere. The atmospheric transmission function T_ν is defined as:

$$T_{\nu}(u(z),\mu_0) = e^{-\int_z^{\infty} k_{\nu}\, du/\mu_o} \tag{2.2}$$

where k_ν is the gas absorption coefficient at frequency ν. The optical depth of a plane parallel atmosphere from top to z can be expressed as:

$$\tau_{\nu}(z) = \int_z^{\infty} k_{\nu}\, du \tag{2.3}$$

The upward diffused radiation flux, then, can be expressed as following:

$$F^{\uparrow}(z) = \mu_0 \int_0^{\infty} \alpha_{sv} S_{0v} T_v(u^*(z),\mu_0)\, dv \qquad (2.4)$$

where α_{sv} is surface albedo, and u^* is the effective total absorber amount traversed by the diffused reflected radiation (Lacis and Hansen, 1974). Therefore, calculations of radiation fluxes can be related to development of the parameterization of transmission functions of various absorbing gases.

2.2 Scattering atmosphere:

In an atmosphere where scattering by clouds and other particles (such as aerosols) is significant, the problem of radiation transfer becomes more complex. We start with the basic radiation transfer equation in a scattering-absorbing atmosphere without consideration of thermal emission:

$$\mu \frac{dI(\tau,\mu,\phi)}{d\tau} = I(\tau,\mu,\phi) - \frac{1}{4\pi} \int_{-1}^{1} \int_{0}^{2\pi} \Phi(\mu,\phi;\mu',\phi')\, I(\tau,\mu',\phi')\, d\phi'\, d\mu' - \frac{S_0}{4\pi} \Phi(\mu,\phi;-\mu_0,\phi_0)\, e^{-\tau/\mu_0} \qquad (2.5)$$

where I is the diffuse radiation intensity along the angles μ and ϕ through an atmospheric path defined by the optical depth τ. Now, $\tau = \tau_s + \tau_a + \tau_g$, which includes both the scattering (τ_s) and

absorption (τ_a) contributions from particles (such as cloud droplets, and aerosols), as well as contributions from absorbing gases (τ_g). $\Phi(\mu,\phi;\mu',\phi')$ is the scattering phase function for radiation scattered from the direction (μ',ϕ') into the direction (μ,ϕ).

The second term of the right hand of equation (2.5) represents the source function due to multi-scattering, and the third term of the right hand of the equation denotes the source function from incoming solar beam with zenith angle θ_o measured from the outward surface normal direction. Here, we have omitted the subscript, ν, for simplicity and defined the positive direction as the outward direction. The phase function is defined as in normalized form:

$$\frac{\omega}{4\pi} \int_{-1}^{1} \int_{0}^{2\pi} \Phi(\mu,\phi;\mu',\phi')\, d\phi'\, d\mu' = 1 \tag{2.6}$$

where ω is the single-scattering albedo, defined as τ_s / τ. For an azimuth independent scattering phase function, Φ can be expressed as:

$$\frac{\omega}{2} \int_{-1}^{1} \Phi(\mu,\mu')\, d\mu' = 1 \tag{2.7}$$

and the asymmetry scattering factor, *g*, is defined by following equation:

$$g = \frac{1}{2} \int_{-1}^{1} \Phi(\mu,1)\, \mu\, d\mu \tag{2.8}$$

A value of $g = \pm 1$ represents the complete forward/backward scattering, and $g = 0$ represents an

isotropic scattering.

Now, define the azimuthal averaged radiation intensity as:

$$I(\tau,\mu) = \frac{1}{2\pi}\int_0^{2\pi} I(\tau,\mu,\phi)\, d\phi \tag{2.9}$$

then equation (2.5) becomes:

$$\mu \frac{dI(\tau,\mu)}{d\tau} = I(\tau,\mu) - \frac{1}{4\pi}\int_{-1}^{1} \Phi(\mu,\mu')\, I(\tau,\mu')\, d\mu' - \frac{S_0}{4\pi}\Phi(\mu,-\mu_0)\, e^{-\tau/\mu_0} \tag{2.10}$$

2.3 Solving radiative transfer equation:

It will be very complex and time consuming to solve equation (2.10) analytically. In applications to a GCM, the major concern, in general, is to obtain the upward and downward radiation fluxes. Thus, a simple method of two-stream approximation is widely adopted in the solar radiation calculation. It starts by defining two diffused radiation streams, an upward (+) flux and a downward (-) flux, as hemispheric integrations:

$$F^{\pm}(\tau) = 2\pi \int_0^1 \mu\, I(\tau,\pm\mu)\, d\mu \tag{2.11}$$

Then the hemispheric integrated equation (2.10) can be parameterized as:

$$\begin{cases} \dfrac{dF^{+}(\tau,\mu_0)}{d\tau} = \gamma_1 F^{+}(\tau,\mu_0) - \gamma_2 F^{-}(\tau,\mu_0) - S_0 \omega \gamma_3 e^{-\tau/\mu_0} \\ \dfrac{dF^{-}(\tau,\mu_0)}{d\tau} = \gamma_2 F^{+}(\tau,\mu_0) - \gamma_1 F^{-}(\tau,\mu_0) + S_0 \omega \gamma_4 e^{-\tau/\mu_0} \end{cases} \tag{2.12}$$

where γ_n are to be determined coefficients. By applying the facts that $\Phi(-\mu,\mu') = \Phi(\mu,-\mu')$ and $\Phi(-\mu,-\mu') = \Phi(\mu,\mu')$, the coefficients γ_3 and γ_4 will satisfy the constraint:

$$\gamma_3 + \gamma_4 = 1 \tag{2.13}$$

The actual expressions of those γ_n will be determined by the approximation method applied to the phase function.

For a plane-parallel atmosphere with an optical depth of τ, Meador and Weaver (1980) showed a formal solution of equations in (2.12) from standard techniques. By satisfying boundary conditions of $F^{+}(\tau,\mu_o) = F^{-}(0,\mu_o) = 0$, and define the reflectance R, and total transmittance T:

$$R(\tau,\mu_0) = \frac{F^{+}(0,\mu_0)}{S_0\mu_0}; \qquad T(\tau,\mu_0) = \frac{F^{-}(\tau,\mu_0)}{S_0\mu_0} + e^{-\tau/\mu_0} \tag{2.14}$$

the results of (2.12) are given as:

$$\begin{aligned} R(\tau,\mu_0) = \frac{\omega}{N}[& (1 - k\mu_0)(\alpha_2 + k\gamma_3) e^{k\tau} \\ & - (1 + k\mu_0)(\alpha_2 - k\gamma_3) e^{-k\tau} - 2k(\gamma_3 - \alpha_2\mu_0) e^{-\tau/\mu_0}] \end{aligned} \tag{2.15}$$

and

$$T(\tau,\mu_0) = e^{-\tau/\mu_0}\left\{1 - \frac{\omega}{N}[(1 + k\mu_0)(\alpha_1 + k\gamma_4)e^{k\tau} - (1 - k\mu_0)(\alpha_1 - k\gamma_4)e^{-k\tau} - 2k(\gamma_4 + \alpha_1\mu_0)e^{-\tau/\mu_0}]\right\} \tag{2.16}$$

where

$$N = (1 - k^2\mu_0^2)[(k + \gamma_1)e^{k\tau} + (k - \gamma_1)e^{-k\tau}] \tag{2.17}$$

and

$$\begin{cases} \alpha_1 = \gamma_1\gamma_4 + \gamma_2\gamma_3 \\ \alpha_2 = \gamma_1\gamma_3 + \gamma_2\gamma_4 \\ k = (\gamma_1^2 - \gamma_2^2)^{\frac{1}{2}} \end{cases} \tag{2.18}$$

In order to resolve those γ coefficients, one needs to find a suitable yet simple enough form of the phase function in equation (2.10). Chandrasekhar (1950) showed a very convenient way by expanding it into Legendre series:

$$\Phi(\mu,\mu') = \omega\sum_l (2l + 1)\psi_l P_l(\mu) P_l(\mu') \tag{2.19}$$

where $P_l(\mu)$ is the lth order Legendre polynomial. In practical applications, one usually take the first several terms of the series as the approximation of the phase function. A widely accepted method introduced by Joseph *et. al* (1976) is called delta-Eddington approximation. It defines the phase function by a Dirac delta function of a forward scattering peak plus a two-term expansion of the Legendre series:

$$\Phi(\mu,\mu') = \omega\,[\,2f\delta_{\mu\mu'} + (1-f)(1+3g^{*}\mu\mu')\,] \tag{2.20}$$

where $f = g^2$ is the forward scattering coefficient, and $g^* = (g - f)/(1 - f)$. After adding the delta function into the phase function, the original form of the radiative transfer equation (2.10) can still be held by taking the corresponding transformations:

$$\begin{cases} \tau \;\rightarrow\; \tau^{*} = (1-\omega f)\,\tau \\ \omega \;\rightarrow\; \omega^{*} = (1-f)\,\omega/(1-\omega f) \\ g \;\rightarrow\; g^{*} = (g-f)/(1-f) \end{cases} \tag{2.21}$$

Thus, the γ-coefficients in equation (2.12) and hence in the solutions (2.15) and (2.16) can be expressed as:

$$\begin{cases} \gamma_1 = \dfrac{1}{4}[7 - \omega^{*}(4 + 3g^{*})] \\ \gamma_2 = -\dfrac{1}{4}[1 - \omega^{*}(4 - 3g^{*})] \\ \gamma_3 = \dfrac{1}{4}(2 - 3g^{*}\mu_0) \end{cases} \tag{2.22}$$

The coefficient γ_4 can be obtained through equation (2.13).

3. Spectral bands and gases absorptions:

In the ultraviolet and visible (UVV) spectral region ($\lambda < 0.7\ \mu$), atmospheric ozone is the main absorber, and a weak water vapor absorption is present in the visible spectrum, see Fig. 1.

Following Chou and Suarez (1999), Table 1 lists the band structure in the UVV part of the solar spectrum ($\lambda < 0.7\ \mu$). A single value of ozone absorption coefficient is assigned to each of the eight bands, and the coefficient of the weak water vapor absorption in the visible band is also included.

The mean transmission functions for ozone and water vapor corresponding to a spectral band with a band width of $\Delta\nu$ can be expressed as:

$$\overline{T}_{\Delta\nu}(w) = e^{-\overline{k}w} \tag{3.1}$$

where $\overline{k}$ is the mean absorption coefficient for the spectral band, and w is the absorber amount. In the visible band, the ozone absorption is enhanced by adding an extra value of 0.0033 $(\text{cm-atm})_{STP}^{-1}$. This small value denotes the effect of ozone absorption in the near infrared (NIR) spectrum. Therefore, no extra computation time will be taken for the ozone absorption in the NIR radiation calculations (Chou and Suarez, 1999).

In the NIR spectral region ($\lambda > 0.7\ \mu$), water vapor is the major atmospheric absorber. As described earlier, the small amount of ozone absorption is folded into the visible spectral band for computational efficiency. To solve the complexity of the varying water vapor absorption coefficient with wavenumber in a scattering atmosphere, Chou and Lee (1996) demonstrated that a high accuracy can be achieved by applying a k-distribution method that requires only ten distinct k-values in each of the NIR spectral bands. Table 2 shows the spectral band structure in NIR region, the k-values chosen, and their corresponding solar flux weighted k-distribution functions for water vapor absorption. In NCEP models, two choices of band structures are

available: a three-band structure offers better accuracy, while a compact one-band structure offers gain in computation speed. The mean transmission function, $\bar{T}$, due to water vapor absorption in a NIR spectrum band with spectral interval $\Delta\nu$ becomes:

$$\overline{T}_{\Delta\nu}(w) = \sum_{i=1}^{n} h_i(p_r, T_r)\, e^{-k_i w} \tag{3.2}$$

where w is the water vapor amount. h_i is the k-distribution function to the corresponding k_i value at a preselected reference pressure, p_r, and a reference temperature, T_r (discussed later), and n = 10 is the total number of k values use in each NIR band.

In additional to the ozone and water vapor absorptions, secondary absorbing gases such as carbon dioxide and oxygen are also included in the calculation, but are treated separately. The reduction of transmission function for the weak absorption by O_2 over a wide spectrum is approximated as Chou and Saurez (1999):

$$\Delta\overline{T}(w_{O_2}) = 1 - e^{-\bar{k}\sqrt{w}} \tag{3.3}$$

where

$$\bar{k} = 0.000145\,(cm-atm)^{-\frac{1}{2}} \tag{3.4}$$

is the mean absorption coefficient, and the solar flux spectral weight for the total O_2 absorption is 0.0633.

Chou and Suarez (1999) noted that the absorption due to CO_2 in solar spectrum overlaps with water vapor. They used two parameterization methods in the calculations to address the difference in overlapping effects. The first one deals with the strong CO_2 absorption in two narrow spectral bands at 4.3 μ and 2.7 μ regions (wavenumber 2200 - 2400 cm^{-1} and 3500 - 3760 cm^{-1}). It is found that the CO_2 absorption in these regions overlaps little with water vapor absorption, thus, an average water vapor path can be comfortably used in the calculation of the reduction in transmission (normalized to the entire solar spectrum) due to CO_2:

$$\Delta\bar{T}(u',p) = \int e^{-\tau_w(p)}(1 - e^{-\tau_c(u',p)})\, S_\nu\, d\nu / \int S_\nu\, d\nu \qquad (3.5)$$

where water vapor path $\tau_w(p)$ is integrated from top of the atmosphere to pressure level p at mean cosine zenith angle value of 0.5, and the CO_2 path is computed by given value of $u' = \rho_c / \mu$, where ρ_c is CO_2 concentration. S_ν denotes the incoming solar flux density at wavenumber ν multiplied by cosine of zenith angle. The values of $\Delta\bar{T}$ are precalculated in a table with u' ranging from 250 to 3300 ppmv in 61 intervals, and $\log_{10}p$ ranging from -2.0 to 3.0 in 100 intervals, where p *is* in mb.

For spectral region outside the two strong bands (4.3 and 2.7 μ), absorption due to CO_2 overlaps strongly with water vapor absorption. Therefore, the reduction in transmission (also normalized to the entire solar spectrum) due to CO_2 is expressed differently as:

$$\Delta\bar{T}(w,u) = \int e^{-k_\nu w}(1 - e^{-\gamma_\nu u})\, S_\nu\, d\nu / \int S_\nu d\nu \qquad (3.6)$$

where scaled absorber amounts w, u, and absorption coefficients k_v, γ_v are for water vapor and CO_2, respectively. The values of $\Delta\bar{T}(w,u)$ are precalculated from a wide range of w and u ($\log_{10}u$ is from -3.0 to 3.3 in 42 even intervals, u in $(\text{cm-atm})_{\text{STP}}$, and $\log_{10}w$ is from -4.0 to 1.4 in 36 intervals, w in g cm^{-2}). Limited extrapolation is applied when values of w and u fall outside those ranges.

To account for variations of absorption coefficients with changing pressure and temperature along vertical atmospheric path, Chou (1986) developed a simple one-parameter scaling method. By choosing a reference temperature, $T = 240$ K, and a reference pressure level, $p_r = 300$ mb (hPa), the pressure and temperature scaling factors f_1 and f_2 are defined as:

$$\begin{cases} f_1(p,p_r) = \left(\dfrac{p}{p_r}\right)^{0.8} \\ \\ f_2(T,T_r) = e^{0.00135(T-T_r)} \end{cases} \tag{3.7}$$

By applying both f_1 and f_2, to the water vapor absorption coefficient, it can be expressed as:

$$k_v(p,T) = k_v(p_r,T_r)\, f_1(p,p_r)\, f_2(T,T_r) \tag{3.8}$$

Since the temperature effect is not as significant as the pressure effect on the absorptions due to O_2 and CO_2, their absorption coefficients are scaled by pressure factor only:

$$k_v(p) = k_v(p_r)\, f_1(p,p_r) \tag{3.9}$$

4. Rayleigh scattering and aerosol effect:

Rayleigh scattering effect is strong in the UVV region of the solar spectrum but weak in the NIR region. The total column optical depth τ_{Ray} for each of the spectral band is derived from data given by Fröhlich and Shaw (1980) (see Table 1 and Table 2). The model layer optical depth is computed by $\tau_R(k) = \tau_{Ray}\, \Delta p(k) / p_s$, where p_s is surface pressure and $\Delta p(k)$ is the pressure thickness of the kth layer.

The optical properties of atmospheric aerosols are computed from a globally distributed aerosol data set with a horizontal resolution of five-degree longitude-latitude (Hess *et al.*, 1998; WMO WCP-112, 1986). Seven typical aerosol vertical distribution profiles are used in the data set. For each of the profiles, up to five distinct vertical atmospheric domains are given according to the geographic region and the type of profile selected. Table 3 lists the type of seven profiles and their corresponding assigned vertical domain boundaries. In the table, the value of model sigma level at the surface is defined as 1.0, and is 0.0 at the top of the atmosphere.

Aerosols are usually a combined mixture of particles of different sources. Different components have different optical properties and relative humidity dependency. Based on Koepke *et al.* (1997), ten different types of aerosol components (Table 4) are used in the construction of aerosol profiles. At each geographic location (a five-degree grid area in the global data set), climatological data of aerosol components are given, including the aerosol profile type, the mixing ratios of the aerosol components, and the mean particle number density,

etc. A detailed discussion of the treatment of model aerosol properties in each of the atmospheric domains is given below.

In the lower atmosphere (atmospheric domain 1), up to five different types of aerosol components (out of a total of ten distinct component types used in the parameterization) are given for each of the five-degree geographic locations. Corresponding climatological values of mixing ratios are also assigned to the components of the mixture. The effective optical properties of the aerosol mixture then can be expressed as:

$$\begin{cases} \delta_\nu = \bar{N} \sum c_i \delta_{\nu_i} \\ \omega_\nu = \sum c_i \omega_{\nu_i} \delta_{\nu_i} \,/\, \sum c_i \delta_{\nu_i} \\ g_\nu = \sum c_i g_{\nu_i} \sigma_{\nu_i} \,/\, \sum c_i \sigma_{\nu_i} \end{cases} \tag{4.1}$$

where c_i is the mixing ratio of the ith aerosol component, δ_{vi}, σ_{vi}, ω_{vi}, and g_{vi} are coefficients for extinction, scattering, single scattering albedo, and asymmetry factor, respectively, for a spectral band v. $\bar{N}$ is the climatological mean value of aerosol particle number density in the domain. Based on the sources of their origin, the ten types of aerosols listed in Table 4 are divided into two groups. The first group includes six of the aerosol types whose optical properties are, in general, not sensitive to the changing of atmospheric humidity. The coefficients for the first group of aerosol components (Hess *et al.,* 1998) are given in Tables 5a - 5d. The second group contains four aerosol types. Those aerosols, on the other hand, may absorb water content in the atmosphere. To account for variations of optical properties of these aerosols due to the changing

of ambient relative humidity, a simple parameterization method is developed by applying regression on the data from Hess *et al.* (1998) as below:

$$\begin{cases} \delta_{v,i} = a_{0_{v,i}} + a_{1_{v,i}} R_0 + a_{2_{v,i}} R_1 \\ \sigma_{v,i} = b_{0_{v,i}} + b_{1_{v,i}} R_0 + b_{1_{v,i}} R_1 \\ \omega_{v,i} = c_{0_{v,i}} + c_{1_{v,i}} R_0 + c_{2_{v,i}} R_2 \\ g_{v,i} = d_{0_{v,i}} + d_{1_{v,i}} R_0 + d_{2_{v,i}} R_2 \end{cases} \tag{4.2}$$

where

$$R_0 = RH - 0.5, \quad R_1 = e^{\gamma_{v,i} R_0}, \quad and \; R_2 = R_0^2 . \tag{4.3}$$

Values of *a, b*, and *c* are given in Table 6a - 6d, and those of γ are given in Table 7. RH denotes the atmospheric relative humidity.

Above the first domain in certain geographic area, there may exist a layer of mineral type aerosol, as designated as MITR in Table 4, which is lifted above the boundary layer by convection and then transported by horizontal wind. The transported mineral from deserts may overlay above oceans (such as that from Sahara over the eastern part of Atlantic ocean), or above continent area (such as that from Gobi desert to mid-west China). This type of aerosol, if exists, is defined in the second domain of the vertical profile, and the climatological value of mean particle number density is used in the calculation.

In the free troposphere, where the third aerosol domain is defined, a prescribed three-

component (INSO, SOOT, and WASO in Table 4) aerosol mixture is used (Hess *et al.*, 1998). The values of mixing ratios of the three components are fixed at 0.00017, 0.4, and 0.59981, respectively. The mean particle number density in this domain is set to be 730 cm^{-3}.

Domain 4 is located in the stratosphere, where the aerosol extinction coefficient, δ, is prescribed (given in Table 7), and the values of single scattering albedo and asymmetry factor are fixed at 0.9 and 0.6, respectively. Above Domain 4 is the upper stratosphere (designated as Domain 5). In the NCEP's application, we assume that no traceable aerosol exist in this domain and above.

The optical depth of aerosol of each model vertical layer is then readily defined as:

$$\begin{cases} \tau_{v,k} = \delta_{v,k} H (e^{-Z_{k+1}/H} - e^{-Z_k/H}) & \text{if } H \geq 0 \\ \tau_{v,k} = \delta_{v,k} \Delta Z_k & \text{otherwise} \end{cases} \tag{4.4}$$

where H is the scale height of aerosols which is listed in Table 3, Z_k and ΔZ_k are height of the kth model level and layer thickness in km, respectively.

$$\Delta Z_k = H_{0_k} [\ln(p_{k+1/2}) - \ln(p_{k-1/2})] \tag{4.5}$$

where H_{0k} is the kth layer's mean atmospheric scale height in km computed by model's hydrostatic equation. p_k is the kth layer mean pressure, and $p_{k+1/2}$ and $p_{k-1/2}$ are the pressure at the interfaces of layer k.

The five-degree resolution of global aerosol composition distribution used in the model is given by Koepke *et al.* (1997). Their data set includes both winter and summer climatological values of aerosol distribution. At NCEP, the data set is interpolated to obtain monthly data with the same horizontal resolution.

5. Cloud optical properties:

Two methods are being used to parameterize cloud radiative properties in the NCEP's models. The first method uses a diagnostic cloud scheme, in which cloud properties are diagnosed from model predicted temperature, pressure, and boundary-layer circulations. Following Harshvardhan *et al.* (1989), the cloud optical depth from the model diagnostic cloud scheme is defined as:

$$\tau_c = \begin{cases} a\,(T_c + 82.5)^2\ \Delta p_c & -82.5^0C \le T_c < -10^0C \\ (b\,T_c + 0.08)\ \Delta p_c & -10^0C \le T_c < 0^0C \\ c\ \Delta p_c & 0^0C \le T_c \end{cases} \qquad (5.1)$$

where T_c is the cloud layer mean temperature, and Δp_c is the pressure thickness of the cloud in mb. The fitting coefficients *a, b*, and *c* are set to be $2.0\text{x}10^{-6}$, $6.949\text{x}10^{-3}$, and 0.08, respectively. In this diagnostic method, cloud single scattering albedo, ω, and asymmetry factor, *g*, are prescribed (see Table 8) but separately for water cloud and ice cloud. The separation temperature is defined at $T_c = -10^0$ *C*.

The second method, which we call here as prognostic cloud scheme, we use explicitly determined condensate to compute cloud radiative properties. For water clouds, cloud optical depth, τ, single scattering albedo, ω, and asymmetry factor, g, are defined as:

$$\begin{cases} \tau_w = LWP\ (a_{0_w} + a_{1_w}/r_{e_w}) \\ 1 - \omega_w = b_{0_w} + b_{1_w} r_{e_w} + b_{2_w} r_{e_w}^2 \\ g_w = c_{0_w} + c_{1_w} r_{e_w} + c_{2_w} r_{e_w}^2 \end{cases} \tag{5.2}$$

where LWP is cloud water path in unit of g/m^2, and r_e is the effective radius of water droplet in unit of μm. The coefficients a, b, and c are given in Table 9(a) and 9(b) . For ice clouds, τ, ω, and g are defined as:

$$\begin{cases} \tau_i = IWP\ (a_{0_i} + a_{1_i}/r_{e_i}) \\ 1 - \omega_i = b_{0_i} + b_{1_i} r_{e_i} + b_{2_i} r_{e_i}^2 \\ g_i = c_{0_i} + c_{1_i} r_{e_i} + c_{2_i} r_{e_i}^2 \end{cases} \tag{5.3}$$

where IWP is cloud ice path, and coefficients a, b, and c are given in Table 9(c) and 9(d).

The parameterization of effective radius, r_e, of water droplet is similar to the method used by Kiehl *et al.* (1998) in the NCAR CCM3. We fix r_e to a value of 10μm over the oceans. Over the land, r_e is defined as:

$$r_e = 5.0 - 0.25 T_c \tag{5.4}$$

Thus, the effective radius of cloud water droplets will reach to a minimum values of 5μm when temperature T_c is above 0^0 C, and to a maximum value of 10μm when T_c becomes colder than -20^0C.

For ice clouds, following Heymsfield and McFarquhar (1996), we have made the effective ice droplet radius to be an empirical function of ice water concentration (IWC) and environmental temperature as:

$$r_{ei} = \begin{cases} (1250/9.917)IWC^{0.109} & T < -50^0C \\ (1250/9.337)IWC^{0.080} & -50^0C \le T < -40^0C \\ (1250/9.208)IWC^{0.055} & -40^0C \le T < -30^0C \\ (1250/9.387)IWC^{0.031} & -30^0C \le T \end{cases} \tag{5.5}$$

where *IWC* and *IWP* satisfy:

$$IWP_{\Delta Z} = \int_{\Delta Z} IWC\, dZ \tag{5.6}$$

6. Radiation flux calculation:

In a plane-parallel atmospheric layer, radiative properties of several absorbing and scattering components (such as water vapor, ozone, Rayleigh scattering, aerosols, and clouds, etc.) are combined to obtain effective (or the bulk) layer properties.

$$\begin{cases} \tau = \sum_i \tau_i \\ \omega = \sum_i \omega_i \tau_i / \sum_i \tau_i \\ g = \sum_i g_i \omega_i \tau_i / \sum_i \omega_i \tau_i \\ f = \sum_i f_i \omega_i \tau_i / \sum_i \omega_i \tau_i \end{cases} \tag{6.1}$$

where $f_i = g_i^2$, except $f_{Ray} = 0.1$. By applying the delta-Eddington transformations in (2.21) to τ, ω, and g, and the γ coefficients in (2.22), the layer reflectance, R, and total transmittance, T, for direct radiation at cosine zenith angle μ_0 can be derived as:

$$\begin{cases} R(\mu_0) = (\alpha - \gamma)te^{-\tau^*/\mu_0} + (\alpha + \gamma)r - (\alpha - \gamma) \\ T(\mu_0) = (\alpha + \gamma)t + (\alpha - \gamma)re^{-\tau^*/\mu_0} - (\alpha + \gamma - 1)e^{-\tau^*/\mu_0} \end{cases} \tag{6.2}$$

where

$$\begin{cases} \alpha = \frac{3}{4}\omega^* \mu_0 [\frac{g + (1 - \omega^* g^*)}{1 - \lambda^2 \mu^2}] \\ \gamma = \frac{1}{2}\omega^* [\frac{1 + 3g^*(1 - \omega^*)\mu^2}{1 - \lambda^2 \mu^2}] \\ \lambda = [3(1 - \omega^*)(1 - \omega^* g^*)]^{1/2} \\ r = [(u+1) + (u+1)e^{-\lambda\tau^*}][(u-1) - (u-1)e^{-\lambda\tau^*}]N^{-1} \\ t = 4ue^{-\lambda\tau^*}N^{-1} \\ N = [(u+1) + (u-1)e^{-\lambda\tau^*}][(u+1) - (u-1)e^{-\lambda\tau^*}] \\ u = \frac{3}{2}\frac{1 - \omega^* g^*}{\lambda} \end{cases} \tag{6.3}$$

Following Chou and Suarez (1999), the layer reflectance and transmittance for diffused radiation are computed by approximating incident solar zenith angle at value of 53^0 ($1/\mu_0 = 1.66$):

$$\begin{cases} \overline{R} = R(\overline{\mu} = \cos(53^0)) \\ \overline{T} = T(\overline{\mu} = \cos(53^0)) \end{cases} \tag{6.4}$$

A two stream adding method is used to combine layers in a column atmosphere. As shown bellow in a two-layer case (layer 1 overlying layer 2), the combined reflectance and the total transmission to direct radiation, and the solar beam transmission are defined as:

$$\begin{cases} R_{12}(\mu_0) = R_1(\mu_0) + \dfrac{\overline{T}_1[(T_1(\mu_0) - T_1^{\downarrow}(\mu_0))\overline{R}_2 + T_1^{\downarrow}(\mu_0)R_2(\mu_0)]}{1 - \overline{R}_1\overline{R}_2} \\ T_{12}(\mu_0) = T_1^{\downarrow}(\mu_0)T_2(\mu_0) + \dfrac{\overline{T}_2[(T_1(\mu_0) - T_1^{\downarrow}(\mu_0)) + T_1^{\downarrow}(\mu_0)R_2(\mu_0)\overline{R}_1]}{1 - \overline{R}_1\overline{R}_2} \\ T_{12}^{\downarrow}(\mu_0) = T_1^{\downarrow}(\mu_0)T_2^{\downarrow}(\mu_0) \end{cases} \tag{6.5}$$

where

$$T_k^{\downarrow}(\mu_0) = e^{-\tau_k^*/\mu_0} \tag{6.6}$$

is the direct solar beam transmission for layer *k*. The combined reflectance to diffused radiation can be expressed in two situations. One is that the upper layer is illuminated by diffused radiation, and the other is that the lower layer is illuminated:

$$\begin{cases} \overline{R}_{+} = \overline{R}_{12} = \overline{R}_1 + \dfrac{\overline{T}_1 \overline{R}_2 \overline{T}_1}{1 - \overline{R}_1 \overline{R}_2} \\ \overline{R}_{-} = \overline{R}_{21} = \overline{R}_2 + \dfrac{\overline{T}_2 \overline{R}_1 \overline{T}_2}{1 - \overline{R}_1 \overline{R}_2} \end{cases} \tag{6.7}$$

By using the two-stream adding method described in Chou and Suarez (1999) and Briegleb (1992), one can obtain normalized fluxes at layer interfaces through two calculation passes. The first pass starts from the top and adds one layer at a time until it reaches the bottom surface. During this pass, the total downward transmission at each level, $T(\mu_0)$, and the diffuse reflectance for layers illuminated from below, $\overline{R}_{-}$, are computed. The second pass starts from the bottom surface and works one layer at a time to the top to obtain the reflectance to the direct radiation, $R(\mu_0)$, at each level, and the diffuse reflectance, $\overline{R}_{+}$, for layers illuminated from above. Thus the normalized upward and downward fluxes at the the lower boundary of layer k are readily available as given below:

$$\begin{cases} F^{\uparrow}_{k+1/2}(\mu_0) = \dfrac{T^{\downarrow}_k(\mu_0) R_{k+1}(\mu_0) + (T_k(\mu_0) - T^{\downarrow}_k(\mu_0)) \overline{R}_{+,k+1}}{1 - \overline{R}_{-,k} \overline{R}_{+,k+1}} \\ F^{\downarrow}_{k+1/2}(\mu_0) = T^{\downarrow}_k(\mu_0) + \dfrac{T^{\downarrow}_k(\mu_0) R_{k+1}(\mu_0) \overline{R}_{-,k} + (T_k(\mu_0) - T^{\downarrow}_k(\mu_0))}{1 - \overline{R}_{-,k} \overline{R}_{+,k+1}} \end{cases} \tag{6.8}$$

At the top of the atmosphere ($k = 1$), then:

$$F^{\uparrow}_{1-1/2}(\mu_0) = R_1(\mu_0) \quad \textit{and} \quad F^{\downarrow}_{1-1/2}(\mu_0) = 1 \tag{6.9}$$

The net flux at layer interface is then computed as:

$$F_{net}(\mu_0) = S_0 \mu_0 \sum_i w_i [F^{\downarrow}(\mu_0) - F^{\uparrow}(\mu_0)] \tag{6.10}$$

where S_0 is the incoming solar flux at the top of the atmosphere, i is the index of spectral band, and w_i is the spectral weight for the corresponding band.

7. Flux calculation in cloudy sky and reduction due to CO_2 and O_2 absorption:

When clouds are present, the atmospheric column is divided into two parts: a clear-sky portion and a cloudy portion. A combined maximum and random cloud overlapping method is developed to calculate the fraction of clear-sky view, A, at layer interfaces. The calculation is started from the top of the atmosphere (level index $k = 1$) and towards down as:

$$A_{k+1/2} = \begin{cases} A_{k-1/2} & \text{if } C_k = 0 \\ A_{k-1/2}(1 - C_k) & \text{if } C_k > 0 \ \& \ C_{k-1} = 0 \\ (1 - \delta) \min(A_{k-1/2}, 1 - C_k) + \delta A_{k-1/2}(1 - C_k) & \text{if } C_k > 0 \ \& \ C_{k-1} > 0 \end{cases} \tag{7.1}$$

where $A_{k\pm1/2}$ are the fraction of clear-sky view at the upper/lower boundaries of layer k, and C_k is the fraction of cloud amount for layer k. The mixing coefficient, δ, between maximum and random overlapping of vertically contiguous clouds is defined as:

$$\delta_k = 2 \frac{|(C_k - C_{k-1}|}{(C_k + C_{k-1})} \tag{7.2}$$

The value range of δ is limited between 0 (totally maximum overlapping) and 1 (totally random overlapping). When the value of δ is small (e.g. the adjacent cloud amounts are similar), then the overlap is tilted towards maximum overlapping. On the other hand, when δ becomes large (e.g. the adjacent clouds because very different), then more weight will be put on the random overlapping. In the current operational GFS model, we fix the value of δ=1 for randomly overlapping clouds.

The fraction of clear-sky view at the surface, A_{sfc}, then is used to normalize cloud amount in the cloudy portion of the atmospheric column:

$$C_k^{'} = \frac{C_k}{C_{tot}} \tag{7.3}$$

where $C_{tot} = 1 - A_{sfc}$ is the effective total cloud amount. The normalized cloud amount $C^{'}$ is used to scale the layer optical depth during radiation calculations in the cloudy portion of the atmosphere. After computing the net radiation fluxes separately for clear-sky ($F_{net-clr}$) and for cloudy-sky ($F_{net-cld}$), reductions of downward fluxes due to O_2 and CO_2, are applied to the net fluxes.

$$\begin{cases} F^{'}_{net-clr}(k) = F_{net-clr}(k) - \Delta F_{clr}(k) \\ F^{'}_{net-cld}(k) = F_{net-cld}(k) - \Delta F_{cld}(k) \end{cases} \tag{7.4}$$

where the reduction of flux in cloudy sky is defined as:

$$\Delta F_{cld}(k) = \begin{cases} \Delta F_{clr}(k) & above\ top\ most\ cloud \\ \Delta F_{clr}(k)\dfrac{F_{net-cld}(k)}{F_{net-clr}(k)} & otherwise \end{cases} \tag{7.5}$$

Finally, the net flux for total sky is a combination of the clear and cloudy sky fluxes:

$$F_{net-tot}(k) = (1 - C_{tot}) F'_{net-clr}(k) + C_{tot} F'_{net-cld}(k) \tag{7.6}$$

The temperature change for layer k due to solar radiation is then calculated from:

$$\frac{dT_k}{dt} = - \frac{g}{C_p} \frac{dF_{net}(k)}{dp} \tag{7.7}$$

where, T is temperature, t is time, g is the gravitational acceleration, and C_p is the heat capacity of air at constant pressure.

8. Surface albedo:

Surface albedo has a strong effect on the surface energy balance as well as the reflected solar radiation by the earth-atmosphere system. In this section, we describe the procedure presently used at NCEP in parameterizing solar radiative transfer. We use a seasonally varying surface albedo data set at one-degree horizontal resolution developed based on Briegleb (1992) and Briegleb et al. (1986). In each of the four seasonal data sets, there are six component data fields. Four of them contain background surface albedos for diffused radiation. These four component albedos are designated as either for a strong type of solar zenith angle dependency or a weak type one in the UVV spectral region ($\lambda \leq 0.7\mu$), and in the NIR region ($\lambda \geq 0.7\mu$), such as $A_{S,UV}$, $A_{W,UV}$, $A_{S,NIR}$, and $A_{W,NIR}$, respectively. The other two components in the data sets contain

fractions of coverage of the surface vegetation types, that show either a strong or a weak zenith angle dependencies (i.e. f_S *or* f_W, and $f_S + f_W \leq 1$).

The four-component surface albedos for diffused radiation in the seasonal data sets are derived from land-use and surface albedo data given by Matthews (1984, 1983). There are 32 different types of surface vegetation listed in Matthews' data. We group the 32 types into 13 model vegetation types shown in Table 10. In addition, any region where human land-use activity is high (e.g. Matthews' cultivation intensity index is higher than 4 in a 0 - 5 scale), a value of 1 is assigned to its model vegetation type. Over desert areas (Matthews' surface index number of 30), on the other hand, data are modified to reflect some brighter area associated with sandy type of cover and other darker area with rocky type of cover. Table 11 lists the seasonal climatological mean values of surface albedos for the 13 surface types. Those values are albedos for diffused solar radiation in the UVV spectrum, and in the NIR spectrum, respectively.

These seasonal data sets are used to obtain the albedo components on the model grid at a given forecast time through spatial and temporal interpolations. In a given model grid, the area is divided into three possible fractions. One is for the snow covered area which includes land and sea ice, f_{snow}, the second is for the open water, f_{sea}, and the last one is for land area without snow covering, f_{land}.

$$f_{land} + f_{sea} + f_{snow} = 1 \tag{8.1}$$

The fraction of snow covered area is defined from model variables of snow depth, surface roughness, (Briegleb, 1992), and adjusted by surface orography over mountains:

$$\begin{cases} f_{snow} = \dfrac{20D}{R + 20D} f_H \\ f_H = (a + bH) \end{cases} \tag{8.2}$$

where the liquid water equivalent snow depth, D, surface roughness, R, and the variance of orography, H, are in meters. The coefficients a and b are set to be 1.0577 and 0.0011538, respectively, and the value of the adjustment f_H is limited between 0.2 and 1. Over the oceans without sea ice (where sea surface temperature is great than $271.2C^0$), the fraction of snow cover is set to zero. The fraction of coverage over land and oceans are then defined as:

$$\begin{cases} f_{land} = (f_S + f_W)(1 - f_{snow}) \\ f_{sea} = (1 - f_S - f_W)(1 - f_{snow}) \end{cases} \tag{8.3}$$

Under direct sun light, different types of surface vegetation exhibit different relationship between direct radiation albedo and solar zenith angles. As shown in Table 10, the first seven surface types (index ranging from 0 to 6) are characterized by a strong zenith angle dependency, while the rest are linked to weak zenith angle dependency. Over land, surface albedos for direct radiation are calculated from their corresponding diffused radiation parts by multiplying a zenith angle dependency function $r(\mu_0)$:

$$\begin{cases} A_S^{dir}(\mu_0) = A_S^{dif} r_S(\mu_0) = A_S^{dif} \dfrac{1.4}{1 + 0.8\mu_0} \\ A_W^{dir}(\mu_0) = A_W^{dif} r_W(\mu_0) = A_W^{dif} \dfrac{1.1}{1 + 0.2\mu_0} \end{cases} \tag{8.4}$$

where μ_0 is the cosine of solar zenith angle, and A_S and A_W are albedos corresponding to the strong and the weak zenith angle dependency, respectively.

Over the oceans, the albedos for diffused radiation in both spectral regions are fixed at 0.06 when sea surface temperature is above 271.5^0K. Following Briegleb et al. (1986), an analytic formula of Payne (1972) data is used to derive the albedo for direct radiation:

$$A_{sea}^{dir}(\mu_0) = \frac{2.6}{\mu_0^{1.7} + 0.065} + 15(\mu_0 - 0.1)(\mu_0 - 0.5)(\mu_0 - 1.0) \tag{8.5}$$

Over sea ice, where temperature is below 271.1^0 K, both the direct and the diffused surface albedos are assigned to a value of 0.7 in the UVV spectrum and 0.65 in the NIR spectrum. A quadratic interpolation is used when sea surface temperature is in between 271.1^0 K and 271.5^0 K:

$$\begin{cases} A_{UVV} = 0.7 - 4.0(T_{sea} - 271.1)^2 \\ A_{NIR} = 0.65 - 3.6875(T_{sea} - 271.1)^2 \end{cases} \tag{8.6}$$

where T_{sea} is sea surface temperature in unit of K.

The diffused part of snow albedo is prescribed as 0.9 for the UVV spectrum, and 0.75 for the NIR spectrum. When snow covers sea ice, the method of Grumbine (1994) is employed:

$$\begin{cases} A_{UVV} = 0.7 - 0.03\,T_g \\ A_{NIR} = 0.6 - 0.03\,T_g \end{cases} \tag{8.7}$$

Where T_g is the ground temperature in ^{0}C. The values will reach to their upper and lower limits when T_g becomes lower than -5 ^{0}C and higher than 0 ^{0}C, respectively. For direct radiation part of snow albedos, the values of the diffused albedos (UVV and NIR) are used for high sun ($\mu_0 >$ 0.5), while a function of zenith angle dependency is added for a low sun condition ($\mu_0 < 0.5$):

$$A_{snow}^{dir}(\mu_0) = A_{snow}^{dif} + \frac{1}{2}(1 - A_{snow}^{dif})\left(\frac{3}{1 + 4\mu_0} - 1\right) \tag{8.8}$$

Finally, the four components (direct and diffused albedos for UVV and NIR spectrums) of total surface albedo for radiation computations are assembled as following:

$$\begin{cases} A_{UVV}^{dif} = A_{land,UVV}^{dif} f_{land} + A_{sea,UVV}^{dif} f_{sea} + A_{snow,UVV}^{dif} f_{snow} \\ A_{UVV}^{dir} = A_{land,UVV}^{dir} f_{land} + A_{sea,UVV}^{dir} f_{sea} + A_{snow,UVV}^{dir} f_{snow} \\ A_{NIR}^{dif} = A_{land,NIR}^{dif} f_{land} + A_{sea,NIR}^{dif} f_{sea} + A_{snow,NIR}^{dif} f_{snow} \\ A_{NIR}^{dir} = A_{land,NIR}^{dir} f_{land} + A_{sea,NIR}^{dir} f_{sea} + A_{snow,NIR}^{dir} f_{snow} \end{cases} \tag{8.9}$$

where

$$\begin{cases} A_{land,UVV}^{dif} = A_{S,UVV}^{dif} f_S + A_{W,UVV}^{dif} f_W \\ A_{land,UVV}^{dir} = A_{S,UVV}^{dir} f_S + A_{W,UVV}^{dir} f_W \\ A_{land,NIR}^{dif} = A_{S,NIR}^{dif} f_S + A_{W,NIR}^{dif} f_W \\ A_{land,NIR}^{dir} = A_{S,NIR}^{dir} f_S + A_{W,NIR}^{dir} f_W \end{cases} \tag{8.10}$$

where f_S and f_W are fractions of cover in a grid cell for strong and weak zenith angle dependencies, respectively.

Acknowledgments. We thank Dr. Ming-Dah Chou for providing documentation of his work on parameterization of solar radiation transfer, and thank Drs. Shi-Keng Yang and Yi Jin for their helpful review comments. We would also thank Dr. Suranjana Saha and many other NCEP researchers for their help on model implementations.

REFERENCES

Briegleb, B. P., 1992: Delta-Eddington approximation for solar radiation in the NCAR community climate model. *J. Geophy. Res.*, **97**, 7603-7612.

Briegleb, B. P., P. Minnis, V. Ramanathan, and E. Harrison, 1986: Comparison of regional clear-sky albedos inferred from satellite observations and model computations. *J. Clim. Appl. Meteor.*, **25**, 214-226.

Chandresekher, S., 1950: Radiative transfer. Dover, 393 pp.

Chou, M.-D., 1986: Atmospheric solar heating rate in the water vapor bands. *J. Clim. Appl. Meteor.*, **25**, 1532-1542.

Chou, M.-D., and K.-T. Lee, 1996: Parameterizations for the absorption of solar radiation by water vapor and ozone. *J. Atmos. Sci.*, **53**, 1203-1208.

Chou, M.-D., and M. Suarez, 1999: A solar radiation parameterization for atmospheric studies. NASA/TM-1999-104606, Vol. **15**, 40 pp.

Coakley, J. A., R. D. Cess, and F. B. Yurevich, 1983: The effect of tropospheric aerosols on the earth's radiation budget: A parameterization for climate models. *J. Atmos. Sci.*, **40**, 116-138.

Fröhlich, C., and G. E. Shaw, 1980: New determination of Rayleigh scattering in the terrestrial atmosphere. *Appl. Opt.*, **19**, 1773-1775.

Fu, Q., 1996: An accurate parameterization of the solar radiative properties of cirrus clouds for climate models. *J. Clim*., **9**, 2058-2082.

Grumbine, R. W., 1994: A sea-ice albedo experiment with the NMC medium range forecast model. *Weather and Forecasting*, **9**, 453-456.

Harshvardhan, D. a. Randall, T. G. Corsetti, and D. A. Dazlich, 1989: Earth radiation budget and cloudiness simulations with a general circulation model. *J. Atmos. Sci.*, **46**, 1922-1942.

Hess, M., P. Koepke, and I. Schult, 1998: Optical properties of aerosols and clouds: The software package OPAC. *Bull. Am. Meteor. Soc.*, **79**, 831-844.

Heymsfield, A. J., and G. M. McFarquhar, 1996: High albedos of cirrus in the tropical Pacific warm pool. *J. Atmos. Sci.*, **53**, 2424-2451.

Kiehl, J. T., J. J. Hack, G. B. Bonan, B. A. Boville, D. L. Willamson, and P. J. Rasch, 1998: The National Center for Atmospheric Research community climate model: CCM3. *J. Clim.*, **11**, 1131-1149.

Koepke, P., M. Hess, I. Schult, and E. P. Shettle, 1997: Global aerosol data set. MPI Meteorologie Hamburg Report No. **243**, 44 pp.

Joseph, J. H., W. j., Wiscombe, and J. A. Weinman, 1976: The delta-Eddington approximation for radiative flux transfer. *J. Atmos. Sci., **33***, 2452-2459.

Lacis, A. A., and J. E. Hansen, 1974: A parameterization for the absorption of solar radiation in the earth's atmosphere. *J. Atmos. Sci., **33***, 118-133.

Matthews, E., 1983: Global vegetation and land use: New high-resolution data bases for climate studies. *J. Clim. Appl. Meteor.*, **22**, 474-487.

Matthews, E., 1984: Vegetation, land-use and seasonal albedo data sets. NASA/TM-1984-86107.

Meador, W. E., and W. R. Weaver, 1980: Two stream approximations to radiative transfer in planetary atmospheres: A unified description of existing methods and a near improvement. *J. Atmos. Sci.*, **37**, 630-643.

Payne, R. E., 1972: Albedo of the sea surface. *J Atmos. Sci.*, **29**, 959-970.

Slingo, A., 1989: A GCM parameterization for the shortwave radiative properties of water clouds. *J. Atmos. Sci.*, **46**, 1419-1427.

Stephens, G. L., 1984: The parameterization of radiation for numerical weather prediction and climate models. *Mon. Wea. Rew.*, **112**, 826-867.

World Meteorological Organization, 1986: A preliminary cloudless standard atmosphere for radiation computation. WCP-112, TD-No. **24**,53 pp.

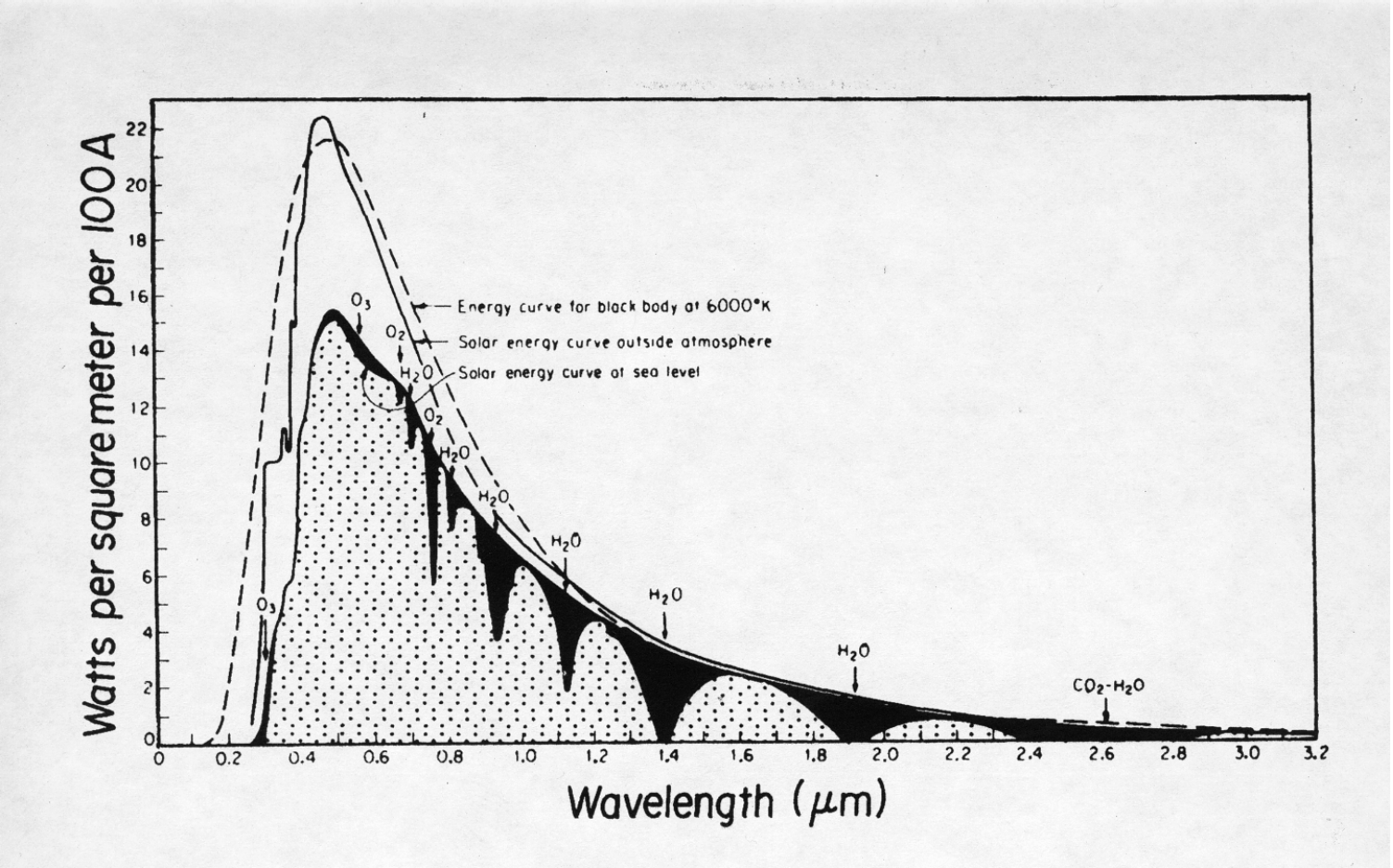

Figure 1. Spectral energy curve of solar radiation at sea level and extrapolated outside the atmosphere The darkened aeras illustrate gases absorption bands while the unshaded area represents Rayleigh scatter effects (from Stephens, 1984)

Table 1. The spectral range, weight, and coefficients for O_3, H_2O absorption (Chou and Suarez, 1999), and Rayleigh scattering Optical depth (Fröhlich and Shaw, 1980) in the ultraviolet and visible bands.

Band	Spectral Range (μm)	Spectral Weight (S/S_0)	K_{O3} $(cm\text{-}atm)^{-1}$	K_{H2O} cm^2g^{-1}	τ_{Ray} Tot Col
UV-C					
1	0.175-0.225	0.00057	30.47	0.00000	7.006
2	0.225-0.245				
	0.260-0.280	0.00367	187.24	0.00000	2.117
3	0.245-0.260	0.00083	301.92	0.00000	2.453
UV-B					
4	0.280-0.295	0.00417	42.83	0.00000	1.398
5	0.295-0.310	0.00600	7.09	0.00000	1.133
6	0.310-0.320	0.00556	1.25	0.00000	.9532
UV-A					
7	0.320-0.400	0.05913	0.0345	0.00000	.6104
PAR (visible)					
8	0.400-0.700	0.39081	0.0572*	0.00075	.1096

* Enhanced by the O_3 absorption in the near infrared spectrum.

Table 2. The spectral range, weight, k-value, distribution function for water vapor (Chou and Lee, 1996), and Rayleigh scattering Optical depth (Fröhlich and Shaw, 1980) in the near infrared bands.

		Three-band			One-band
Band		1	2	3	
Spectral Range (μm)		2.27-10.0	1.22-2.27	0.70-1.22	0.70-10.0
τ_{Ray} Tot Col		0.000289	0.00375	0.0354	0.0128
Spectral Weight(S/S_0)		(0.04235)	(0.16536)	(0.32055)	(0.52926)
k-value(cm^2g^{-1})		Flux-weighted k-distribution function			
1	0.0010	0.01074	0.08236	0.20673	0.29983
2	0.0133	0.00360	0.01157	0.03497	0.05014
3	0.0422	0.00411	0.01133	0.03011	0.04555
4	0.1334	0.00421	0.01143	0.02260	0.03824
5	0.4217	0.00389	0.01240	0.01336	0.02965
6	1.3340	0.00326	0.01258	0.00696	0.02280
7	5.6230	0.00499	0.01381	0.00441	0.02321
8	31.620	0.00465	0.00650	0.00115	0.01230
9	177.80	0.00245	0.00244	0.00026	0.00515
10	1000.0	0.00145	0.00094	0.00000	0.00239

Table 3. Model Aerosol profile and domain structure

Aerosol Profile Type	Model sigma level of domain upper boundary and Aerosol Scale Height H				
	1	2	3	4	5
1 Antarctic(ANT)	0.261	_	0.193	0.0058	0.0
	8.0km		8.0km	0.0km	0.0km
2 Arctic (ARC)	0.785	_	0.193	0.0058	0.0
	0.0km		8.0km	0.0km	0.0km
3 Continent(CNT)	0.785	_	0.193	0.0058	0.0
	8.0km		8.0km	0.0km	0.0km
4 Maritime (MAR)	0.785	_	0.193	0.0058	0.0
	1.0km		8.0km	0.0km	0.0km
5 Desert (DES)	0.463	_	0.193	0.0058	0.0
	2.0km		8.0km	0.0km	0.0km
6 Maritime with mineral overlay (MARME)	0.785	0.648	0.193	0.0058	0.0
	1.0km	0.0km	8.0km	0.0km	0.0km
7 Continent with mineral overlay (CNTME)	0.785	0.648	0.193	0.0058	0.0
	8.0km	0.0km	8.0km	0.0km	0.0km

Table 4. Model Aerosol Components

Type of aerosol component		Relative humidity dependency
1 Water-insoluble	(INSO)	No
2 Soot	(SOOT)	No
3 Mineral nuc mode	(MINM)	No
4 Mineral acc mode	(MIAM)	No
5 Mineral coa mode	(MICM)	No
6 Mineral transported	(MITR)	No
7 Water-soluble	(WASO)	Yes
8 Sea salt acc mode	(SSAM)	Yes
9 Sea salt coa mode	(SSCM)	Yes
10 Sulfate droplets	(SUSO)	Yes

Table 5. Coefficients of Aerosol Components
Without Relative Humidity Dependency

(5a) Extinction Coefficient δ:

Band	INSO	SOOT	MINM	MIAM	MICM	MITR
8-band UV and VIS spectrum						
1	8.052e-03	1.356e-06	1.032e-04	2.821e-03	7.597e-02	5.445e-03
2	8.076e-03	1.313e-06	1.023e-04	2.835e-03	7.608e-02	5.465e-03
3	8.060e-03	1.342e-06	1.029e-04	2.826e-03	7.601e-02	5.452e-03
4	8.112e-03	1.248e-06	1.010e-04	2.857e-03	7.625e-02	5.496e-03
5	8.148e-03	1.173e-06	9.940e-05	2.879e-03	7.641e-02	5.527e-03
6	8.156e-03	1.154e-06	9.895e-05	2.884e-03	7.645e-02	5.534e-03
7	8.282e-03	8.612e-07	9.008e-05	2.969e-03	7.703e-02	5.650e-03
8	8.524e-03	5.432e-07	6.925e-05	3.140e-03	7.811e-02	5.876e-03
1-band NIR spectrum						
1	8.823e-03	2.132e-07	2.628e-05	3.325e-03	8.214e-02	6.442e-03
3-band NIR spectrum						
1	6.435e-03	7.664e-08	3.429e-06	2.452e-03	9.026e-02	6.150e-03
2	9.062e-03	1.471e-07	1.413e-05	3.365e-03	8.368e-02	6.691e-03
3	9.021e-03	2.626e-07	3.506e-05	3.411e-03	8.040e-02	6.348e-03

(5b) Scattering Coefficient σ:

Band	INSO	SOOT	MINM	MIAM	MICM	MITR
8-band UV and VIS spectrum						
1	4.447e-03	4.177e-07	8.264e-05	1.625e-03	4.142e-02	3.034e-03
2	4.723e-03	4.061e-07	8.314e-05	1.662e-03	4.150e-02	3.080e-03
3	4.539e-03	4.138e-07	8.281e-05	1.637e-03	4.145e-02	3.049e-03
4	5.136e-03	3.887e-07	8.389e-05	1.718e-03	4.162e-02	3.149e-03
5	5.404e-03	3.623e-07	8.453e-05	1.795e-03	4.184e-02	3.252e-03
6	5.423e-03	3.540e-07	8.464e-05	1.817e-03	4.192e-02	3.285e-03
7	5.729e-03	2.301e-07	8.277e-05	2.178e-03	4.367e-02	3.840e-03
8	6.255e-03	1.129e-07	6.675e-05	2.750e-03	5.242e-02	4.909e-03
1-band NIR spectrum						
1	7.253e-03	1.972e-08	2.546e-05	3.119e-03	6.317e-02	5.886e-03
3-band NIR spectrum						
1	5.553e-03	7.201e-10	2.423e-06	2.140e-03	6.357e-02	5.264e-03
2	7.757e-03	6.464e-09	1.348e-05	3.178e-03	6.539e-02	6.172e-03
3	7.229e-03	2.859e-08	3.417e-05	3.205e-03	6.186e-02	5.805e-03

(5c) Single Scattering Albedo ω:

Band	INSO	SOOT	MINM	MIAM	MICM	MITR
8-band UV and VIS spectrum						
1	5.524e-01	3.081e-01	8.004e-01	5.760e-01	5.452e-01	5.571e-01
2	5.846e-01	3.095e-01	8.125e-01	5.860e-01	5.455e-01	5.634e-01
3	5.631e-01	3.086e-01	8.044e-01	5.793e-01	5.453e-01	5.592e-01
4	6.329e-01	3.116e-01	8.307e-01	6.011e-01	5.459e-01	5.728e-01
5	6.631e-01	3.084e-01	8.509e-01	6.230e-01	5.476e-01	5.884e-01
6	6.647e-01	3.061e-01	8.560e-01	6.298e-01	5.483e-01	5.935e-01
7	6.918e-01	2.672e-01	9.189e-01	7.336e-01	5.670e-01	6.797e-01
8	7.336e-01	2.025e-01	9.651e-01	8.748e-01	6.708e-01	8.345e-01
1-band NIR spectrum						
1	8.228e-01	7.671e-02	9.463e-01	9.367e-01	7.693e-01	9.133e-01
3-band NIR spectrum						
1	8.612e-01	8.972e-03	7.039e-01	8.739e-01	7.035e-01	8.567e-01
2	8.565e-01	4.103e-02	9.460e-01	9.438e-01	7.816e-01	9.224e-01
3	8.009e-01	1.024e-01	9.733e-01	9.395e-01	7.693e-01	9.142e-01

(5d) Asymmetry Factor g:

Band	INSO	SOOT	MINM	MIAM	MICM	MITR
8-band UV and VIS spectrum						
1	9.390e-01	5.020e-01	7.320e-01	9.030e-01	9.460e-01	9.310e-01
2	9.219e-01	4.873e-01	7.272e-01	8.946e-01	9.469e-01	9.256e-01
3	9.333e-01	4.971e-01	7.304e-01	9.002e-01	9.463e-01	9.292e-01
4	8.963e-01	4.653e-01	7.200e-01	8.820e-01	9.482e-01	9.175e-01
5	8.798e-01	4.468e-01	7.126e-01	8.668e-01	9.484e-01	9.064e-01
6	8.787e-01	4.437e-01	7.109e-01	8.627e-01	9.481e-01	9.031e-01
7	8.600e-01	3.960e-01	6.880e-01	8.030e-01	9.400e-01	8.500e-01
8	8.280e-01	3.306e-01	6.616e-01	7.342e-01	8.923e-01	7.742e-01
1-band NIR spectrum						
1	8.045e-01	1.937e-01	5.688e-01	6.920e-01	8.282e-01	7.110e-01
3-band NIR spectrum						
1	8.989e-01	7.289e-02	3.909e-01	6.921e-01	8.067e-01	7.122e-01
2	8.136e-01	1.494e-01	5.319e-01	6.878e-01	8.103e-01	6.977e-01
3	7.864e-01	2.302e-01	6.087e-01	6.942e-01	8.406e-01	7.178e-01

Table 6. Coefficients of Aerosol Components With Relative Humidity dependency

(6a) Mapping Coefficients a_0, a_1, and a_2 for the Extinction Coefficient δ:

Band	WASO			SSCM			SSAM			SUSO		
	a_0	a_1	a_2	a_0	a_1	a_2	a_0	a_1	a_2	a_0	a_1	a_2
8-band UV and VIS spectrum												
1	1.595e-5	1.330e-5	4.237e-10	2.304e-3	2.784e-3	1.272e-09	1.448e-1	1.770e-1	9.004e-08	2.309e-4	2.389e-4	7.845e-10
2	1.528e-5	1.268e-5	4.174e-10	2.320e-3	2.798e-3	1.275e-09	1.451e-1	1.773e-1	9.000e-08	2.302e-4	2.409e-4	7.955e-10
3	1.573e-5	1.310e-5	4.216e-10	2.309e-3	2.789e-3	1.273e-09	1.449e-1	1.771e-1	9.003e-08	2.307e-4	2.396e-4	7.882e-10
4	1.426e-5	1.176e-5	4.079e-10	2.344e-3	2.820e-3	1.279e-09	1.455e-1	1.778e-1	8.994e-08	2.292e-4	2.440e-4	8.120e-10
5	1.331e-5	1.090e-5	3.976e-10	2.368e-3	2.842e-3	1.282e-09	1.458e-1	1.782e-1	8.997e-08	2.272e-4	2.461e-4	8.286e-10
6	1.312e-5	1.073e-5	3.951e-10	2.374e-3	2.848e-3	1.283e-09	1.459e-1	1.782e-1	9.000e-08	2.265e-4	2.462e-4	8.322e-10
7	1.011e-5	8.090e-6	3.512e-10	2.468e-3	2.964e-3	1.291e-09	1.470e-1	1.805e-1	8.984e-08	2.115e-4	2.436e-4	8.894e-10
8	6.646e-6	5.898e-6	6.175e-11	2.609e-3	3.191e-3	1.322e-09	1.485e-1	1.805e-1	9.088e-08	1.718e-4	2.079e-4	9.422e-10
1-band NIR spectrum												
1	2.007e-6	1.856e-6	9.589e-12	2.439e-3	3.323e-3	1.496e-09	1.553e-1	1.868e-1	9.237e-08	7.643e-5	1.000e-4	1.695e-10
3-band NIR spectrum												
1	4.815e-7	8.023e-7	3.772e-12	1.482e-3	2.153e-3	1.589e-09	1.673e-1	1.966e-1	9.462e-08	2.483e-5	3.554e-5	1.950e-11
2	9.357e-7	7.900e-7	5.441e-12	2.246e-3	3.217e-3	1.599e-09	1.580e-1	1.893e-1	9.297e-08	4.494e-5	6.263e-5	3.156e-11
3	2.732e-6	2.527e-6	1.241e-11	2.666e-3	3.547e-3	1.433e-09	1.524e-1	1.844e-1	9.179e-08	9.999e-5	1.327e-4	1.971e-10

(6b) Mapping Coefficients b_0, b_1, and b_2 for the Scattering Coefficient σ:

Band	WASO			SSCM			SSAM			SUSO		
	b_0	b_1	b_2	b_0	b_1	b_2	b_0	b_1	b_2	b_0	b_1	b_2
8-band UV and VIS spectrum												
1	1.431e-5	1.314e-5	4.229e-10	2.303e-3	2.784e-3	1.272e-09	1.448e-1	1.771e-1	8.997e-08	2.309e-4	2.389e-4	7.845e-10
2	1.400e-5	1.257e-5	4.168e-10	2.319e-3	2.798e-3	1.275e-09	1.451e-1	1.774e-1	8.996e-08	2.302e-4	2.409e-4	7.955e-10
3	1.421e-5	1.295e-5	4.209e-10	2.309e-3	2.789e-3	1.273e-09	1.449e-1	1.772e-1	8.997e-08	2.307e-4	2.396e-4	7.882e-10
4	1.355e-5	1.172e-5	4.077e-10	2.344e-3	2.820e-3	1.279e-09	1.455e-1	1.779e-1	8.993e-08	2.292e-4	2.440e-4	8.120e-10
5	1.294e-5	1.091e-5	3.976e-10	2.368e-3	2.843e-3	1.282e-09	1.458e-1	1.782e-1	8.997e-08	2.272e-4	2.461e-4	8.286e-10
6	1.276e-5	1.074e-5	3.951e-10	2.374e-3	2.848e-3	1.283e-09	1.459e-1	1.782e-1	9.000e-08	2.265e-4	2.462e-4	8.322e-10
7	9.919e-6	8.093e-6	3.512e-10	2.468e-3	2.964e-3	1.291e-09	1.470e-1	1.805e-1	8.984e-08	2.115e-4	2.436e-4	8.894e-10
8	6.505e-6	5.900e-6	6.173e-11	2.609e-3	3.191e-3	1.322e-09	1.485e-1	1.805e-1	9.088e-08	1.718e-4	2.079e-4	9.422e-10
1-band NIR spectrum												
1	1.848e-6	1.798e-6	9.430e-12	2.411e-3	3.277e-3	1.467e-09	1.507e-1	1.814e-1	8.835e-08	7.545e-5	9.867e-5	1.674e-10
3-band NIR spectrum												
1	1.224e-7	1.088e-7	1.425e-12	1.088e-3	1.420e-3	1.191e-09	1.223e-1	1.253e-1	6.140e-08	9.093e-6	1.152e-5	1.221e-11
2	8.152e-7	7.708e-7	5.416e-12	2.240e-3	3.214e-3	1.588e-09	1.542e-1	1.867e-1	8.824e-08	4.481e-5	6.249e-5	3.148e-11
3	2.570e-6	2.513e-6	1.240e-11	2.665e-3	3.547e-3	1.432e-09	1.518e-1	1.844e-1	9.171e-08	9.999e-5	1.327e-4	1.971e-10

(6c) Mapping Coefficients c_0, c_1, and c_2 for the Single Scattering Albedo ω:

Band	WASO			SSCM			SSAM			SUSO		
	c_0	c_1	c_2	c_0	c_1	c_2	c_0	c_1	c_2	c_0	c_1	c_2
8-band UV and VIS spectrum												
1	8.820e-1	1.329e-1	8.925e-2	9.999e-1	2.130e-4	4.523e-5	9.994e-1	1.319e-3	-8.368e-4	1.000e+0	0.000e+0	0.000e+0
2	9.071e-1	1.059e-1	6.894e-2	9.999e-1	1.776e-4	-2.168e-5	9.995e-1	1.062e-3	-6.559e-4	1.000e+0	0.000e+0	0.000e+0
3	8.904e-1	1.239e-1	8.248e-2	9.999e-1	2.012e-4	2.292e-5	9.994e-1	1.233e-3	-7.760e-4	1.000e+0	0.000e+0	0.000e+0
4	9.449e-1	6.534e-2	3.848e-2	1.000e+0	1.244e-4	-1.202e-4	9.997e-1	6.763e-4	-3.884e-4	1.000e+0	0.000e+0	0.000e+0
5	9.684e-1	3.971e-2	1.988e-2	1.000e+0	7.586e-5	-1.400e-4	9.998e-1	3.888e-4	-2.249e-4	1.000e+0	0.000e+0	0.000e+0
6	9.697e-1	3.814e-2	1.904e-2	1.000e+0	6.654e-5	-1.230e-4	9.999e-1	3.521e-4	-2.188e-4	1.000e+0	0.000e+0	0.000e+0
7	9.790e-1	2.712e-2	1.340e-2	1.000e+0	0.000e+0	0.000e+0	1.000e+0	0.000e+0	0.000e+0	1.000e+0	0.000e+0	0.000e+0
8	9.742e-1	3.376e-2	1.754e-2	1.000e+0	0.000e+0	0.000e+0	1.000e+0	0.000e+0	0.000e+0	1.000e+0	0.000e+0	0.000e+0
1-band NIR spectrum												
1	8.678e-1	1.263e-1	1.084e-1	9.842e-1	-1.268e-2	1.762e-2	9.728e-1	-1.375e-2	-1.121e-2	9.651e-1	1.992e-2	1.374e-2
3-band NIR spectrum												
1	4.741e-1	-2.284e-2	4.737e-1	7.713e-1	-2.185e-1	3.434e-1	7.285e-1	-2.238e-1	2.247e-1	4.767e-1	2.866e-1	2.205e-1
2	8.438e-1	1.973e-1	1.269e-1	9.962e-1	5.396e-4	-7.588e-3	9.782e-1	-7.483e-3	-5.631e-2	9.936e-1	4.980e-3	6.300e-4
3	9.198e-1	1.049e-1	6.285e-2	9.995e-1	1.023e-3	-7.783e-4	9.960e-1	7.559e-3	-4.647e-3	1.000e+0	-1.103e-7	-1.787e-6

(6d) Mapping Coefficients d_0, d_1, and d_2 for the Asymmetry Factor g:

Band	WASO			SSCM			SSAM			SUSO		
	d_0	d_1	d_2	d_0	d_1	d_2	d_0	d_1	d_2	d_0	d_1	d_2
8-band UV and VIS spectrum												
1	7.240e-1	8.256e-2	3.256e-2	7.758e-1	1.140e-1	1.584e-2	8.495e-1	2.280e-2	-1.158e-1	7.431e-1	7.601e-2	-1.690e-2
2	7.178e-1	9.182e-2	3.936e-2	7.739e-1	1.174e-1	1.304e-2	8.500e-1	2.590e-2	-1.115e-1	7.470e-1	7.510e-2	-2.346e-2
3	7.220e-1	8.564e-2	3.483e-2	7.752e-1	1.151e-1	1.491e-2	8.497e-1	2.383e-2	-1.144e-1	7.444e-1	7.571e-2	-1.909e-2
4	7.085e-1	1.057e-1	4.957e-2	7.710e-1	1.225e-1	8.826e-3	8.507e-1	3.054e-2	-1.052e-1	7.527e-1	7.373e-2	-3.331e-2
5	7.013e-1	1.156e-1	5.817e-2	7.681e-1	1.260e-1	7.093e-3	8.505e-1	3.608e-2	-9.727e-2	7.574e-1	7.191e-2	-3.971e-2
6	7.003e-1	1.167e-1	5.963e-2	7.674e-1	1.263e-1	7.395e-3	8.502e-1	3.756e-2	-9.510e-2	7.581e-1	7.138e-2	-4.017e-2
7	6.851e-1	1.307e-1	8.454e-2	7.614e-1	1.239e-1	4.612e-3	8.486e-1	5.475e-2	-6.403e-2	7.681e-1	6.680e-2	-4.495e-2
8	6.554e-1	1.454e-1	1.182e-1	7.606e-1	1.143e-1	-2.758e-2	8.424e-1	6.848e-2	-4.633e-2	7.632e-1	8.161e-2	-2.990e-2
1-band NIR spectrum												
1	5.476e-1	1.640e-1	2.019e-1	7.725e-1	1.059e-1	-7.896e-2	8.272e-1	9.706e-2	-2.339e-2	6.906e-1	1.454e-1	6.351e-2
3-band NIR spectrum												
1	3.633e-1	1.483e-1	2.637e-1	7.303e-1	1.911e-1	8.386e-3	8.526e-1	1.819e-1	-1.123e-1	5.014e-1	2.269e-1	2.352e-1
2	5.068e-1	1.733e-1	2.345e-1	7.797e-1	1.068e-1	-9.434e-2	8.157e-1	1.042e-1	4.413e-3	6.629e-1	1.697e-1	1.018e-1
3	5.899e-1	1.605e-1	1.771e-1	7.728e-1	9.568e-2	-8.258e-2	8.304e-1	8.425e-2	-3.121e-2	7.264e-1	1.228e-1	2.347e-2

Table 7. Power Coefficient γ for Aerosols in Troposphere, and Extinction Coefficient δ for Aerosols in Stratosphere

Band	γ WASO	SSAM	SSCM	SUSO	δ
8-band UV and VIS spectrum					
1	24.0	33.0	33.0	28.0	3.39e-4
2	24.0	33.0	33.0	28.0	3.34e-4
3	24.0	33.0	33.0	28.0	3.38e-4
4	24.0	33.0	33.0	28.0	3.28e-4
5	24.0	33.0	33.0	28.0	3.22e-4
6	24.0	33.0	33.0	28.0	3.18e-4
7	24.0	33.0	33.0	28.0	3.01e-4
8	27.0	33.0	33.0	28.0	2.09e-4
1-band NIR spectrum					
1	29.0	33.0	33.0	31.0	7.72e-5
3-band NIR spectrum					
1	29.0	33.0	33.0	34.0	1.70e-5
2	29.0	33.0	33.0	34.0	5.01e-5
3	29.0	33.0	33.0	31.0	1.03e-4

Table 8. Single Scattering Albedo and Asymmetry Factor for Water and Ice Clouds in the Diagnostic Cloud Scheme

Band	water cloud ω	g	ice cloud ω	g
8-band UV+VIS spectrum				
all	.999998	0.8530	.999995	0.7998
1-band NIR spectrum				
1	0.9916	0.8311	0.9750	0.8174
3-band NIR spectrum				
1	0.7570	0.8723	0.7368	0.9070
2	0.9868	0.8182	0.9485	0.8304
3	0.9998	0.8354	0.9995	0.8067

Table 9. Coefficients of cloud radiative parameterization. The top two panels are used in the early 28-layer model. (a) for water cloud derived from data by Slingo (1989), and (b) for ice cloud derived from data by FU (1996). The lower two panels are for the later 64-layer model. (c) for water cloud and (d) for ice cloud. Those values are obtained from Chou and Suarez (1999) and later update, except in the 1-band NIR spectrum that are derived from the 3-band data.

(a) water cloud, 28-layer model

Band	a_0	a_1	b_0	b_1	b_2	c_0	c_1	c_2
8-band UV and VIS spectrum								
all	2.798e-2	1.309e+0	-1.810e-7	1.778e-7	0.0	8.272e-1	2.565e-3	0.0
1-band NIR spectrum								
1	2.517e-2	1.386e+0	3.218e-3	5.217e-4	0.0	7.808e-1	5.031e-3	0.0
3-band NIR spectrum								
1	1.528e-2	1.611e+0	1.674e-1	7.561e-3	0.0	8.344e-1	3.797e-3	0.0
2	2.286e-2	1.449e+0	5.427e-4	1.263e-3	0.0	7.501e-1	6.812e-3	0.0
3	2.642e-2	1.353e+0	-3.306e-6	2.287e-5	0.0	7.922e-1	4.323e-3	0.0

(b) ice cloud, 28-layer model

Band	a_0	a_1	b_0	b_1	b_2	c_0	c_1	c_2
8-band UV and VIS spectrum								
all	-5.975e-6	2.517e+0	1.721e-7	9.177e-8	-1.125e-11	7.480e-1	1.015e-3	-1.531e-6
1-band NIR spectrum								
1	-2.456e-5	2.521e+0	7.083e-3	3.495e-4	-8.500e-7	7.566e-1	1.241e-3	-3.804e-6
3-band NIR spectrum								
1	2.712e-4	2.489e+0	1.738e-1	1.887e-3	-6.615e-6	8.414e-1	1.477e-3	-6.403e-6
2	-4.308e-5	2.523e+0	2.461e-3	9.436e-4	-2.107e-6	7.566e-1	1.537e-3	-5.130e-6
3	-3.917e-5	2.522e+0	-8.979e-7	8.102e-6	-1.862e-10	7.519e-1	1.097e-3	-3.070e-6

(c) water cloud, 64-layer model

Band	a_0	a_1	b_0	b_1	b_2	c_0	c_1	c_2
8-band UV and VIS spectrum								
all	-6.590e-3	1.650e+0	0.0	0.0	0.0	8.256e-1	5.290e-3	-1.487e-4
1-band NIR spectrum								
1	-1.166e-2	1.751e+0	1.040e-4	3.930e-4	-5.686e-6	7.847e-1	9.316e-3	-2.587e-4
3-band NIR spectrum								
1	-3.390e-2	2.160e+0	1.209e-2	1.785e-2	-3.691e-4	8.353e-1	2.572e-3	5.519e-5
2	-1.660e-2	1.850e+0	-1.993e-4	8.876e-4	-6.500e-6	7.451e-1	1.370e-2	-3.820e-4
3	-1.010e-2	1.720e+0	7.150e-8	8.450e-6	-4.150e-8	7.937e-1	8.324e-3	-2.326e-4

(d) ice cloud, 64-layer model

Band	a_0	a_1	b_0	b_1	b_2	c_0	c_1	c_2
8-band UV and VIS spectrum								
all	0.0	1.640e+0	0.0	0.0	0.0	7.462e-1	2.820e-3	-2.300e-5
1-band NIR spectrum								
1	0.0	1.640e+0	2.710e-3	5.977e-4	-2.804e-6	7.250e-1	4.002e-3	-3.264e-5
3-band NIR spectrum								
1	0.0	1.640e+0	4.828e-2	5.470e-3	-3.618e-5	7.710e-1	4.900e-3	-4.010e-5
2	0.0	1.640e+0	1.120e-3	1.129e-3	-3.580e-6	7.170e-1	4.560e-3	-3.544e-5
3	0.0	1.640e+0	1.410e-6	1.144e-5	-5.000e-9	7.250e-1	3.700e-3	-3.090e-5

Table 10. Surface Vegetation Type And Conversion Table

Type Index	Surface Type Description	Solar Zenith Angle Dependency	Matthews Surface Type
0	Ocean	strong	0
1	Mixed farming, tall grassland	strong	32, culti inten > 75%
2	Tall/medium grassland,evergreen shrubland	strong	17,18,24,26,27
3	Short grassland,meadow and shrubland	strong	19,21,25,28,29
4	Tundra	strong	20,22
5	Sandy desert	strong	30
6	Rocky desert	strong	30
7	Tropical evergreen broadleaved forest	weak	1,2,3
8	Evergreen forest (needleleaved)	weak	4,5,7,8
9	Medium/tall grassland, woodland	weak	6,12,13,14,15,16,23
10	Deciduous forest	weak	9,11
11	Mixed deciduous, evergreen forest	weak	10
12	Ice (land)	weak	31
13	Snow	weak	--

Table 11. Seasonal Values of Diffused Surface Albedos for the UVV and NIR Spectrums

Surface Type	Albedos for Diffused Radiation (UVV/NIR) Winter	Spring	Summer	Fall
0	.06/.06	.06/.06	.06/.06	.06/.06
1	.09/.28	.10/.30	.11/.32	.10/.30
2	.11/.32	.12/.35	.13/.38	.12/.35
3	.14/.33	.15/.36	.16/.39	.15/.36
4	.15/.30	.13/.28	.12/.26	.13/.28
5	.36/.51	.36/.51	.36/.51	.36/.51
6	.25/.40	.25/.40	.25/.40	.25/.40
7	.07/.24	.07/.24	.07/.24	.07/.24
8	.07/.24	.07/.24	.07/.24	.07/.24
9	.06/.28	.07/.30	.08/.32	.07/.30
10	.06/.31	.07/.33	.08/.35	.07/.33
11	.06/.27	.07/.29	.08/.31	.07/.29
12	.90/.65	.90/.65	.90/.65	.90/.65
13	.90/.75	.90/.75	.90/.75	.90/.75